ADJOINT WALL FUNCTIONS: VALIDATION AND APPLICATION TO VEHICLE AERODYNAMICS

EVANGELOS M. PAPOUTSIS-KIACHAGIAS[*], KYRIAKOS C. GIANNAKOGLOU[*] AND C. OTHMER[†]

[*] National Technical University of Athens
Iroon Polytechniou 9, 157 80 Athens, Greece
e-mail: vaggelisp@gmail.com, kgianna@central.ntua.gr,
web page: http://velos0.ltt.mech.ntua.gr/research/

[†] Volkswagen AG, Group Research, Vehicle Technology,
Letter Box 1777, 38436 Wolfsburg, Germany
e-mail: carsten.othmer@volkswagen.de

Key words: Continuous Adjoint Method, Adjoint Wall Functions, Shape Sensitivities, Vehicle Aerodynamics

Abstract. This paper presents the continuous adjoint method for computing the sensitivity derivatives of integral functions used in incompressible aerodynamics; the formulation includes the full differentiation of the Spalart-Allmaras turbulence model, based on wall functions. The development of the continuous adjoint method for this turbulence model with wall functions is presented for the first time; the only previous work on adjoint wall functions was presented by the same group for the k-ϵ model, [12]. Isolated airfoil cases are initially studied, in order to assess the accuracy of the adjoint method which differentiates the turbulence model equations and the law of the wall. Then, the developed method is used to compute drag sensitivity maps of a passenger car.

1 Introduction

In aerodynamic shape optimization, discrete and continuous adjoint methods are in widespread use for computing the derivatives of an objective function with respect to (w.r.t.) the design variables; their advantages and disadvantages are discussed in [4, 6].

Regarding turbulent flows, the majority of published continuous adjoint methods rely on the "frozen turbulence" assumption, i.e. all variations in turbulent quantities w.r.t. the design variables are neglected. This is not, usually, the case in discrete adjoint where the turbulence model equations are often differentiated, [1, 7]. In the continuous adjoint method this paper is dealing with, there are just a few recent papers on the differentiation of the turbulence model PDEs. The first paper on the continuous adjoint to turbulence

models was [11], where the adjoint to the low-Reynolds number variant of the Spalart–Allmaras turbulence model for incompressible flows was presented. Later on, this was extended to compressible flows, [2]. In [12], the adjoint approach to the high-Re $k - \epsilon$ turbulence model with wall functions was formulated by introducing the adjoint friction velocity and the so-called *adjoint wall functions*. The theory and implementation of [12] were based on an in-house, vertex-centered finite-volume code, using the pseudo-compressibility method. There, the implementation of the primal wall functions was based on a slip velocity condition, since the real solid wall was assumed to lie at a distance underneath the grid boundary.

Here, the notion of the adjoint wall functions is expanded and applied to the high-Re number Spalart–Allmaras model for incompressible flows. The cell-centered, pressure-based implementation of the aforementioned model, as programmed in OpenFOAM$^{©}$, is the basis of the adjoint formulation. A no-slip velocity condition is imposed on the wall boundaries along with the law of the wall, expressed by a single formula governing both the viscous sublayer and the logarithmic part of the boundary layer, [3].

The proposed method for computing adjoint-based sensitivities is validated against the outcome of finite differences (FD) in flows around isolated airfoils. Then, the implemented software is used to compute the drag sensitivity map over the surface of a passenger car. In addition, a comparison is conducted between the sensitivity maps obtained by using or avoiding the "frozen turbulence" assumption.

2   Flow Model

The flow model consists of the Navier–Stokes equations for incompressible fluids coupled with the Spalart–Allmaras turbulence model, [9]. The primal PDEs are

$$R^p = -\frac{\partial v_j}{\partial x_j} = 0 \tag{1a}$$

$$R_i^v = v_j \frac{\partial v_i}{\partial x_j} - \frac{\partial}{\partial x_j} \left[(\nu + \nu_t) \left(\frac{\partial v_i}{\partial x_j} + \frac{\partial v_j}{\partial x_i} \right) \right] + \frac{\partial p}{\partial x_i} = 0 \quad , \quad i = 1, 2(, 3) \tag{1b}$$

$$R^{\widetilde{\nu}} = v_j \frac{\partial \widetilde{\nu}}{\partial x_j} - \frac{\partial}{\partial x_j} \left[\left(\nu + \frac{\widetilde{\nu}}{\sigma} \right) \frac{\partial \widetilde{\nu}}{\partial x_j} \right] - \frac{c_{b2}}{\sigma} \left(\frac{\partial \widetilde{\nu}}{\partial x_j} \right)^2 - \widetilde{\nu} \, P\left(\widetilde{\nu} \right) + \widetilde{\nu} \, D\left(\widetilde{\nu} \right) = 0 \tag{1c}$$

where p is the static pressure divided by the constant density, v_i the velocity components, ν the constant bulk viscosity, $\nu_t = \widetilde{\nu} f_{v_1}$ the turbulent viscosity and $\widetilde{\nu}$ the turbulence state variable. The production and dissipation terms are given by $P(\widetilde{\nu}) = c_{b1} \widetilde{Y}$, $D(\widetilde{\nu}) = c_{w1} f_w(\widetilde{Y}) \frac{\widetilde{\nu}}{\Delta^2}$, where $\widetilde{Y} = Y f_{v_3} + \frac{\widetilde{\nu}}{\Delta^2 \kappa^2} f_{v_2}$, $Y = \left| e_{ijk} \frac{\partial v_k}{\partial x_j} \right|$. Y stands for the vorticity magnitude, Δ is the distance of cell-centres from the nearest wall boundaries and e_{ijk} the Levi-Civita symbol. The turbulence model functions are $f_{v_1} = \frac{\chi^3}{\chi^3 + c_{v_1}^3}, f_{v_2} = \frac{1}{\left(1 + \frac{\chi}{c_{v_2}} \right)^3}, f_{v_3} = \frac{(1 + \chi f_{v1})}{c_{v2}} \left[3 \left(1 + \frac{\chi}{c_{v2}} \right) + \left(\frac{\chi}{c_{v2}} \right)^2 \right] \left(1 + \frac{\chi}{c_{v2}} \right)^{-3}, \chi = \frac{\widetilde{\nu}}{\nu}, f_w = g \left(\frac{1 + c_{w_3}^6}{g^6 + c_{w_3}^6} \right)^{1/6} , g = r + c_{w_2}(r^6 - r), r = $

$\frac{\widetilde{\nu}}{\widetilde{Y}\kappa^2\Delta^2}$. The model constants are $c_{b1}=0.1355$, $c_{b2}=0.622$, $\kappa=0.41$, $\sigma=2/3$, $c_{w1}=\frac{c_{b1}}{\kappa^2}+\frac{(1+c_{b2})}{\sigma}$, $c_{w2}=0.3$, $c_{w3}=2$, $c_{v1}=7.1$ and $c_{v2}=5$. To implement the wall function technique, a special treatment of v_i and ν_t on the boundary faces (such as the bottom face in fig. 1) is required. The wall function technique, as programmed in OpenFOAM$^©$, is based on a single formula modeling both the viscous sublayer and the logarithmic region of the turbulent boundary layer [3]
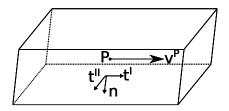
$$f_{WF}=y^+ - v^+ - e^{-\kappa B}\left[e^{\kappa v^+} - 1 - \kappa v^+ - \frac{(\kappa v^+)^2}{2} - \frac{(\kappa v^+)^3}{6}\right]=0 \tag{2}$$

where $\kappa=0.41$ and $B=5.5$. The non-dimensional distance and velocity at cell-centre P are $y_P^+ = \frac{\Delta^P v_\tau}{\nu}$, $v_P^+ = \frac{|v_i|^P}{v_\tau}$ and the friction velocity is computed by

$$v_\tau^2 = -\left[(\nu + \nu_t)\left(\frac{\partial v_i}{\partial x_j} + \frac{\partial v_j}{\partial x_i}\right)\right]^f n_j t_i^I \tag{3}$$

where n_j and t_i^I are shown in fig. 1.

Figure 1: Typical finite volume adjacent to the wall coinciding with the lower face, where **n** is the outwards normal unit vector, $\mathbf{t}^I$ is parallel to the velocity vector at the first cell centre P and $t_i^{II}=e_{ijk}n_j t_k^I$. The bottom face (symbol f) is the boundary face where the no-slip condition is applied.

Using the wall functions technique, $v_i^f = 0$ (no-slip condition) and the viscous flux for the i-th momentum equation at the wall boundary face f is given by

$$-\left[(\nu+\nu_t)\left(\frac{\partial v_i}{\partial x_j}+\frac{\partial v_j}{\partial x_i}\right)\right]^f n_j \approx -\left[(\nu+\nu_t)\frac{\partial v_i}{\partial x_j}\right]^f n_j = -\left(\nu+\nu_t^f\right)\frac{v_i^f - v_i^P}{|Pf|} \tag{4}$$

However, such a finite-difference quotient on a coarse mesh is inconsistent; so the normal velocity gradient in eq. 4 is corrected by computing and using an "artificial" ν_t^f, so that the wall shear stress satisfying eq. 2 and that computed by eq. 4, be equal. As a consequence, in the flow equations, the wall function technique is implemented in the form of $f_{WF}(v_\tau, |v_i|^P, \Delta^P)=0$ (eq. 2 at each face f) which is solved for v_τ and, then, eq. 3 adjusts ν_t^f accordingly. Practically,

$$\nu_t^f = -\frac{v_\tau^2}{\left(\frac{\partial v_i}{\partial x_j} + \frac{\partial v_j}{\partial x_i}\right)^f n_j t_i^I} - \nu \approx -|Pf|\frac{v_\tau^2}{(v_i^f - v_i^P)t_i^I} - \nu = |Pf|\frac{v_\tau^2}{v_i^P t_i^I} - \nu \tag{5}$$

which is, then, used to compute the contribution of the boundary viscous flux to the momentum balance at the first cell adjacent to the wall, eq. 4.

3   Objective Function and its Derivatives

An objective function F comprising only surface integrals can be expressed as

$$F = \int_S F_{S,i} n_i dS \tag{6}$$

where S is the boundary of the computational domain Ω. Differentiating F w.r.t. the design variables $b_n, n \in [1, N]$, yields

$$\frac{\delta F}{\delta b_n} = \int_S \frac{\delta F_{S_i}}{\delta b_n} n_i dS + \int_S F_{S_i} \frac{\delta n_i}{\delta b_n} dS + \int_S F_{S_i} n_i \frac{\delta(dS)}{\delta b_n} \tag{7}$$

In eq. 7, $\delta(\cdot)/\delta b_n$ denotes the total derivative w.r.t. the design variables. We also define the partial derivative $\partial(\cdot)/\partial b_n$ as the variation caused purely by variations in the flow variables (in turn, caused by geometry deformations) without considering space deformations. Any small surface deformation can be seen as a normal perturbation, [5], and the total and partial derivatives of an arbitrary variable Φ w.r.t. b_n written along S are linked through

$$\frac{\delta_s \Phi}{\delta b_n} = \frac{\partial \Phi}{\partial b_n} + \frac{\partial \Phi}{\partial x_k} n_k \frac{\delta x_m}{\delta b_n} n_m \tag{8}$$

By taking into consideration eq. 8 with F_{S_i} instead of Φ and applying the chain rule, eq. 7 can be written as

$$\frac{\delta F}{\delta b_n} = \int_S \frac{\partial F_{S_i}}{\partial v_k} n_i \frac{\partial v_k}{\partial b_n} dS + \int_S \frac{\partial F_{S_i}}{\partial p} n_i \frac{\partial p}{\partial b_n} dS + \int_S \frac{\partial F_{S_i}}{\partial \widetilde{\nu}} n_i \frac{\partial \widetilde{\nu}}{\partial b_n} dS + \int_S \frac{\partial F_{S_i}}{\partial \tau_{kj}} n_i \frac{\partial \tau_{kj}}{\partial b_n} dS$$
$$+ \int_{S_{W_p}} n_i \frac{\partial F_{S_i}}{\partial x_m} n_m \frac{\delta x_k}{\delta b_n} n_k dS + \int_{S_{W_p}} F_{S_i} \frac{\delta n_i}{\delta b_n} dS + \int_{S_{W_p}} F_{S_i} n_i \frac{\delta(dS)}{\delta b_n} \tag{9}$$

where $\tau_{kj} = (\nu + \nu_t)\left(\frac{\partial v_k}{\partial x_j} + \frac{\partial v_j}{\partial x_k}\right)$. The boundary S is written as $S = S_I \cup S_O \cup S_W \cup S_{W_p}$ with S_I, S_O, S_W and S_{W_p} standing for the inlet, outlet, fixed and parameterized wall boundaries of Ω, respectively. Since only S_{W_p} is allowed to vary, quantities related to geometry variations are defined only along S_{W_p}. Eq. 7 includes $\partial F_{S,i}/\partial \widetilde{\nu}$, taking into consideration a possible direct dependence of F on the turbulence model variable. Such a dependence would be ignored if the "frozen turbulence" assumption was made.

4   Development of the Continuous Adjoint Method

Starting point for the derivation of the adjoint equations is the augmented objective function, defined by adding the volume integrals of the primal equations, multiplied by the corresponding adjoint variable fields, to F, as follows

$$F_{aug} = F + \int_\Omega u_i R_i^v d\Omega + \int_\Omega q R^p d\Omega + \int_\Omega \widetilde{\nu}_a R^{\widetilde{\nu}} d\Omega \tag{10}$$

4

where u_i are the adjoint velocity components, q the adjoint pressure and $\widetilde{\nu}_a$ the adjoint to $\widetilde{\nu}$. The latter is omitted in the "frozen turbulence" assumption.

By differentiating eq. 10 w.r.t. b_n and employing the Leibniz theorem for integrals with variable boundaries, we get

$$\frac{\delta F_{aug}}{\delta b_n} = \frac{\delta F}{\delta b_n} + \int_\Omega u_i \frac{\partial R_i^v}{\partial b_n} d\Omega + \int_\Omega q \frac{\partial R^p}{\partial b_n} d\Omega + \int_\Omega \widetilde{\nu}_a \frac{\partial R^{\widetilde{\nu}}}{\partial b_n} d\Omega + \int_{S_{W_p}} \left(u_i R_i^v + q R^p + \widetilde{\nu}_a R^{\widetilde{\nu}} \right) n_k \frac{\delta x_k}{\delta b_n} dS \tag{11}$$

The development of the partial derivatives of the mean flow and turbulence model equations is presented in detail in [11], there for the low-Re number variant of the Spalart–Allmaras model. Since this lengthy development is identical in both variants of the model, it will not be repeated herein.

4.1 Field Adjoint Equations

After taking into consideration the development presented in [11] and the general expression for $\delta F/\delta b_n$, eq. 9, the following form of $\delta F_{aug}/\delta b_n$ is obtained

$$\begin{aligned}
\frac{\delta F_{aug}}{\delta b_n} = &\int_S \mathcal{BC}_i^u \frac{\partial v_i}{\partial b_n} dS + \int_S \left(u_j n_j + \frac{\partial F_{S_i}}{\partial p} n_i \right) \frac{\partial p}{\partial b_n} dS + \int_S \mathcal{BC}^{\widetilde{\nu_a}} \frac{\partial \widetilde{\nu}}{\partial b_n} dS \\
&+ \int_S \left(-u_i n_j + \frac{\partial F_{S_k}}{\partial \tau_{ij}} n_k \right) \frac{\partial \tau_{ij}}{\partial b_n} dS - \int_S \widetilde{\nu}_a \left(\nu + \frac{\widetilde{\nu}}{\sigma} \right) \frac{\partial}{\partial b_n} \left(\frac{\partial \widetilde{\nu}}{\partial x_j} \right) n_j dS \\
&+ \int_\Omega R_i^u \frac{\partial v_i}{\partial b_n} d\Omega + \int_\Omega R^q \frac{\partial p}{\partial b_n} d\Omega + \int_\Omega R^{\widetilde{\nu_a}} \frac{\partial \widetilde{\nu}}{\partial b_n} d\Omega + \int_\Omega \widetilde{\nu} \widetilde{\nu}_a \mathcal{C}_\Delta \frac{\partial \Delta}{\partial b_n} d\Omega \\
&+ \int_{S_{W_p}} n_i \frac{\partial F_{S_{W_p,i}}}{\partial x_m} n_m \frac{\delta x_k}{\delta b_n} n_k dS + \int_{S_{W_p}} F_{S_{W_p,i}} \frac{\delta (n_i dS)}{\delta b_n} + \int_{S_{W_p}} \left(u_i R_i^v + q R^p + \widetilde{\nu}_a R^{\widetilde{\nu}} \right) \frac{\delta x_k}{\delta b_n} n_k dS \tag{12}
\end{aligned}$$

where

$$\mathcal{BC}_i^u = u_i v_j n_j + (\nu + \nu_t) \left(\frac{\partial u_i}{\partial x_j} + \frac{\partial u_j}{\partial x_i} \right) n_j - q n_i + \widetilde{\nu}_a \widetilde{\nu} \frac{\mathcal{C}_Y}{Y} e_{mjk} \frac{\partial v_k}{\partial x_j} e_{mli} n_l + \frac{\partial F_{S_k}}{\partial v_i} n_k \tag{13}$$

$$\mathcal{BC}^{\widetilde{\nu_a}} = \widetilde{\nu}_a v_j n_j + \left(\nu + \frac{\widetilde{\nu}}{\sigma} \right) \frac{\partial \widetilde{\nu}_a}{\partial x_j} n_j - \frac{\widetilde{\nu}_a}{\sigma} (1 + 2 c_{b_2}) \frac{\partial \widetilde{\nu}}{\partial x_j} n_j + \frac{\partial F_{S_k}}{\partial \widetilde{\nu}} n_k \tag{14}$$

Zeroing the multipliers of $\partial v_i/\partial b_n, \partial p/\partial b_n$ and $\partial \widetilde{\nu}/\partial b_n$ in the volume integrals of eq. 12

leads to the field adjoint equations, namely

$$R^q = -\frac{\partial u_j}{\partial x_j} = 0 \tag{15a}$$

$$R_i^u = u_j \frac{\partial v_j}{\partial x_i} - \frac{\partial (v_j u_i)}{\partial x_j} - \frac{\partial}{\partial x_j}\left[(\nu+\nu_t)\left(\frac{\partial u_i}{\partial x_j}+\frac{\partial u_j}{\partial x_i}\right)\right] + \frac{\partial q}{\partial x_i}$$
$$+ \widetilde{\nu}_a \frac{\partial \widetilde{\nu}}{\partial x_i} - \frac{\partial}{\partial x_l}\left(\widetilde{\nu}_a \widetilde{\nu}\frac{\mathcal{C}_Y}{Y}e_{mjk}\frac{\partial v_k}{\partial x_j}e_{mli}\right) = 0 \ , \ \ i=1,2(,3) \tag{15b}$$

$$R^{\widetilde{\nu}_a} = -\frac{\partial(v_j \widetilde{\nu}_a)}{\partial x_j} - \frac{\partial}{\partial x_j}\left[\left(\nu+\frac{\widetilde{\nu}}{\sigma}\right)\frac{\partial \widetilde{\nu}_a}{\partial x_j}\right] + \frac{1}{\sigma}\frac{\partial \widetilde{\nu}_a}{\partial x_j}\frac{\partial \widetilde{\nu}}{\partial x_j} + 2\frac{c_{b2}}{\sigma}\frac{\partial}{\partial x_j}\left(\widetilde{\nu}_a \frac{\partial \widetilde{\nu}}{\partial x_j}\right) + \widetilde{\nu}_a \widetilde{\nu}\mathcal{C}_{\widetilde{\nu}}$$
$$+ \frac{\partial \nu_t}{\partial \widetilde{\nu}}\frac{\partial u_i}{\partial x_j}\left(\frac{\partial v_i}{\partial x_j}+\frac{\partial v_j}{\partial x_i}\right) + (-P+D)\widetilde{\nu}_a = 0 \tag{15c}$$

Eq. 15a is the adjoint continuity equation. The last two terms in the adjoint momentum equations, eqs. 15b, result from the differentiation of the turbulence model equation. This term depends on the adjoint turbulence variable $\widetilde{\nu}_a$, i.e. the solution of the adjoint turbulence model PDE, eq. 15c.

The last integral in eq. 12, containing the distance variation w.r.t. the design variables, is considered to be negligible compared to the rest of the terms comprising eq. 12. The adjoint boundary conditions are formulated by appropriately treating the surface integrals in eq. 12, containing variations in the flow variables.

4.2 Adjoint Boundary Conditions – Adjoint Wall Functions

At S_I and S_O, the adjoint boundary conditions coincide with those presented in [11]. Since the distinguishing feature of the present paper is the use of wall functions, only the adjoint wall boundary conditions are presented.

Since S_W is fixed, the partial and total derivatives of any flow quantity are identical and the total derivatives of the normal and tangent unit vectors are zero. Due to the Dirichlet condition imposed on $\widetilde{\nu}$, the third integral on the r.h.s. of eq. 12, written along S_W vanishes automatically. To make eq. 12 independent of $\frac{\partial}{\partial b_n}\left(\frac{\partial \widetilde{\nu}}{\partial x_j}\right)n_j$, a zero Dirichlet condition is imposed on $\widetilde{\nu}_a$. To eliminate the dependency of $\delta F_{aug}/\delta b_n$ on $\partial p/\partial b_n$, the normal adjoint velocity must be equal to $u_{\langle n\rangle} = -\frac{\partial F_{S_{W,i}}}{\partial p}n_i$. By further developing the first and fourth integrals on the r.h.s. of eq. 12, a Dirichlet condition for $u_{\langle t\rangle}^{II}$ results, along with the following expression

$$u_\tau^2 = (\nu+\nu_t)\left(\frac{\partial u_i}{\partial x_j}+\frac{\partial u_j}{\partial x_i}\right)n_j t_i^I = 0 \tag{16}$$

which stands for the *adjoint friction velocity*. Its role is similar to that of the primal friction velocity, i.e. is used to calculate the adjoint viscous flux in order to complete the

adjoint momentum equilibrium at the first cell adjacent to S_W, fig. 1. The adjoint friction velocity is an indispensable part of the adjoint system of equations to the high-Re Spalart–Allmaras model since, due to the "long distance" between f and P, fig. 1, differentiating normal to the wall is prone to important errors. The implications of neglecting the *adjoint law of the wall* are discussed in section 5.

Since the primal boundary conditions for the S_W and S_{W_p} boundaries are identical, the adjoint boundary conditions for S_{W_p} are the same as those imposed along the S_W boundaries. The only difference is that since S_{W_p} may vary, the total and partial derivatives of the flow quantities are different and linked through eq. 8. In addition, the total variations in the normal and tangent surface vectors are not zero, contributing thus extra terms to the sensitivity derivatives.

4.3   Sensitivity Derivatives

After satisfying the field adjoint equations and their boundary conditions, the remaining terms on the r.h.s. of eq. 12 comprise the sensitivity derivatives expression, which reads

$$\frac{\delta F_{aug}}{\delta b_n} = T_{SD}^{WF} - \int_{S_{W_p}} \mathcal{SD}_1 \frac{\partial \tau_{ij}}{\partial x_m} n_j t_i^I n_m n_k \frac{\delta x_k}{\delta b_n} dS - \int_{S_{W_p}} \mathcal{SD}_1 \tau_{ij} \frac{\delta(n_j t_i^I)}{\delta b_n} dS + \int_{S_{W_p}} \mathcal{SD}_{2,i} v_{\langle t \rangle}^I \frac{\delta t_i^I}{\delta b_n} dS$$

$$- \int_{S_{W_p}} \mathcal{SD}_{2,i} \frac{\partial v_i}{\partial x_m} n_m n_k \frac{\delta x_k}{\delta b_n} dS - \int_{S_{W_p}} \left[\left(\nu + \frac{\widetilde{\nu}}{\sigma} \right) \frac{\partial \widetilde{\nu}_a}{\partial x_j} n_j + \frac{\partial F_{S_z}}{\partial \widetilde{\nu}} n_z \right] \frac{\partial \widetilde{\nu}}{\partial x_m} n_m n_k \frac{\delta x_k}{\delta b_n} dS$$

$$+ T_D + \int_{S_{W_p}} (u_i R_i^v + q R^p + \widetilde{\nu}_a R^{\widetilde{\nu}}) \frac{\delta x_k}{\delta b_n} n_k dS \tag{17}$$

where $\mathcal{SD}_1 = -u_{\langle t \rangle}^I + \phi_{\langle t^I \rangle \langle n \rangle} + \phi_{\langle n \rangle \langle t^I \rangle}$, $\mathcal{SD}_{2,i} = (\nu + \nu_t) \left(\frac{\partial u_i}{\partial x_j} + \frac{\partial u_j}{\partial x_i} \right) n_j - q n_i + \frac{\partial F_{S_{W_p,k}}}{\partial v_i} n_k$ and $\phi_{ij} = \frac{\partial F_{S_{W_p,k}}}{\partial \tau_{ij}} n_k$. In eq. 17, T_{SD}^{WF} results from the differentiation of the law of the wall. T_D is a lengthy expression including variations in geometrical quantities.

5   Validation – Applications

The objective function, to be minimized, is the force exerted on the surface of the aerodynamic body, projected on a predefined direction, **r**. This is written as

$$F = \int_{S_{W_p}} \left[-(\nu + \nu_t) \left(\frac{\partial v_i}{\partial x_j} + \frac{\partial v_j}{\partial x_i} \right) + p \delta_i^j \right] n_j r_i dS \tag{18}$$

5.1   Validation in 2D airfoil cases

In the first one, a symmetric NACA0012 airfoil is parameterized using Bézier–Bernstein polynomials with 12 control points for each of its pressure and suction sides, fig. 2. A hybrid grid with ≈ 200000 cells was generated with a mean non-dimensional distance of

the first cell adjacent to the wall equal to $y^+ \approx 10$. The flow Reynolds number is $Re = 6 \times 10^6$ based on the airfoil chord length and the infinite flow angle is $\alpha_\infty = 3^o$. The proposed method for computing sensitivity derivatives using the adjoint wall functions technique is used to obtain the sensitivities of the drag force (eq. 18 with $\mathbf{r} = [cos(\alpha_\infty), sin(\alpha_\infty)]^T$) exerted on the airfoil w.r.t. the (x, y) coordinates of the 24 control points, resulting to a total of 48 design variables. The outcome of this computation is compared with the result of FD and other alternatives based on the adjoint approach in fig. 3. A detailed description and comments on the performed comparison can be found in the caption of fig. 3.
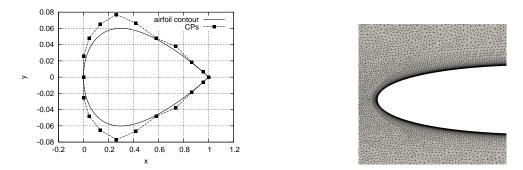

Figure 2: NACA0012, $\alpha_\infty = 3^o$: Airfoil contour and Bézier control points, not in scale, (left) along with a blow-up view of the mesh near the leading edge (right).

In the second case, a NACA4415 airfoil is parameterized using Bézier–Bernstein polynomials with 8 control points on each side, fig. 4. A hybrid grid of about 200000 cells is used with a mean $y^+ \approx 10$. The Reynolds number and infinite flow angle are $Re = 6 \times 10^6$ and $\alpha_\infty = 10^o$, respectively, resulting to mild flow separation close to the trailing edge. For this case as well, the validation of drag sensitivity derivatives is conducted by comparing the outcome of the adjoint wall functions method with FD, fig. 5-left. Even in the presence of mild flow separation, the two methods produce results which are in very good agreement. In fig. 5–right, the same curves are compared with other adjoint-based approaches, reconfirming the observations made in the first case.

5.2   Drag Sensitivity Maps on the Volkswagen Polo car

In this section, the developed software is used to compute the sensitivity derivatives of the drag objective function w.r.t. the normal displacement on the boundary wall nodes of the Volkswagen Polo car (drag sensitivity map). The computational mesh consists of approximately 8 million cells and has an average y^+ value of ≈ 50. The primal flow fields used for the solution of the adjoint equations are obtained by time-averaging the solution of the Navier-Stokes equations, coupled with the DES Spalart–Allmaras model, [10], with wall functions. The time-averaged primal velocity is, then, fed to the RANS-version of the Spalart–Allmaras turbulence model in order to solve for the turbulent viscosity ν_t.
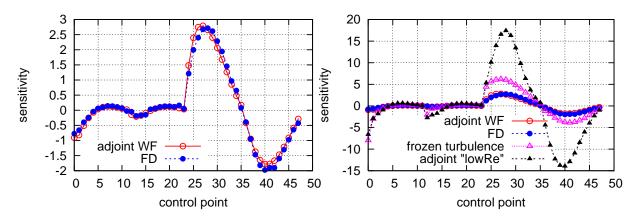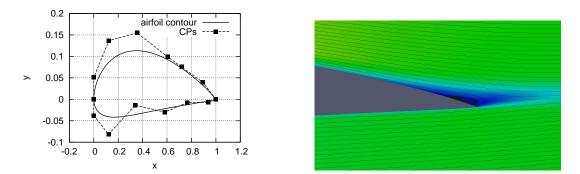
Figure 3: NACA0012, $\alpha_\infty = 3^o$: Left: Drag sensitivities computed using the proposed method (marked as "adjoint WF") are compared to the outcome of FD. The first 24 points correspond to the derivatives w.r.t. the x coordinates of the suction and pressure side control points while the last 24 to those w.r.t. the y coordinates. The two curves are in excellent agreement. Right: The afore-mentioned curves are compared with those resulting from the adjoint method using the "frozen turbulence" assumption and the adjoint method with the "low–Reynolds" approach (different scale on the vertical axis). The latter implies that the turbulence model is differentiated but the differentiation of the wall functions is disregarded (in other words, the primal solver is the high–Re variation of the Spalart–Allmaras model but the adjoint is based on the low–Re variant of the same model; no adjoint wall functions are used). The gain in accuracy through the use of the adjoint wall functions is obvious. In this case, the "low–Re" approach performs even worse than the adjoint method with the "frozen turbulence" assumption, i.e. the incomplete differentiation of the turbulence model produces worse results than the complete omission of its differentiation.

Figure 4: NACA4415 airfoil, $\alpha_\infty = 10^o$: Left: airfoil contour and Bézier–Bernstein control points parameterizing its shape (not in scale). Right: velocity isolines and streamtraces in the vicinity of the trailing edge.

With these fields – time-averaged primal velocity and pressure as well as the RANS-ν_t – the steady-state adjoint equations, presented in sections 4.1 and 4.2, are subsequently solved to obtain the sensitivity derivatives. This procedure has already been used in the past to generate drag sensitivity maps for entire car shapes [8], using however the
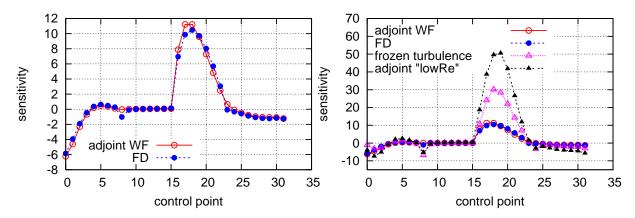
Figure 5: NACA4415 airfoil, $\alpha_\infty = 10^o$: Left: Drag sensitivities computed using the proposed method, compared with FD, notation as in fig. 3. For this case, too, the results of the proposed method match those of FD. Right: The comparison with the adjoint method using the "frozen turbulence" assumption and the "low–Reynolds" approach confirms the observations made in the first case.

"frozen turbulence" assumption. It is now the first time that such sensitivity maps are computed with full differentiation of the turbulence model including adjoint wall functions. Fig. 6 compares sensitivities computed utilizing the two approaches. It can be observed that while the full differentiation of the turbulence model and the "frozen turbulence" assumption compute the same sensitivity sign for almost the entire surface of the car, the latter tends to overestimate the sensitivity magnitude by more than one order of magnitude. In other words, qualitatively, both approaches convey similar messages: the necessity of a rear spoiler for further drag reduction, the beneficial effect of an earlier separation at the rear sides of the car, and of a less pronounced styling of the front wing. For quantitative assessments, i.e. how much drag reduction can be achieved for a given deformation of the car shape, which is a crucial question within the aerodynamic car design process, the sensitivity map based on the "frozen turbulence" assumption proves to be unreliable and the usage of adjoint wall function is a must.

6   Summary–Conclusions

In this paper, the mathematical development of the adjoint wall functions technique, formulated for the one-equation Spalart–Allmaras turbulence model was analyzed. The so-computed drag sensitivity derivatives were validated in two airfoil flow problems and are shown to be in very good agreement with finite-differences. Finally, the developed adjoint software was used to compute the drag sensitivity maps on the surface of a passenger car (with a DES primal solver, followed by averaging) and the computed sensitivities were compared with those obtained by using the "frozen turbulence" assumption. It was observed that the sensitivity sign computed by the two methods was the same for the largest part of the car shape, though the "frozen turbulence"-based sensitivities were at

least one order of magnitude higher than those computed by the proposed method.

REFERENCES

[1] WK. Anderson and DL. Bonhaus. Airfoil design on unstructured grids for turbulent flows. *AIAA Journal*, 37(2):185–191, 1999.

[2] A. Bueno-Orovio, C. Castro, F. Palacios, and E. ZuaZua. Continuous adjoint approach for the SpalartAllmaras model in aerodynamic optimization. *AIAA Journal*, 50(3):631–646, 2012.

[3] NT. Frink. Assessment of an unstructured-grid method for predicting 3-d turbulent viscous flows. *AIAA Paper*, 02(92), 1996.

[4] M. Giles and N. Pierce. An introduction to the adjoint approach to design. *Flow, Turbulence and Combustion*, 65:393–415, 2000.

[5] P. Grinfield. Hadamard's formula inside and out. *Journal of optimization theory and applications*, 146:654–690, 2010.

[6] S. Nadarajah and A. Jameson. Studies of the continuous and discrete adjoint approaches to viscous automatic aerodynamic shape optimization. *AIAA Paper*, 25(30), 2001.

[7] EJ. Nielsen, J. Lu, MA. Park MA, and DL. Darmofal. An implicit exact dual adjoint solution method for turbulent flows on unstructured grids. *Computers & Fluids*, 33:1131–1155, 2004.

[8] C. Othmer. Adjoint methods for car aerodynamics. In *17th European Conference on Mathematics for Industry (to be published in the ECMI special online issue of J. Math. Ind., 2014)*, Lund, Sweden, July 2012.

[9] P. Spalart and S. Allmaras. A one-equation turbulence model for aerodynamic flows. *AIAA Paper*, 04(39), 1992.

[10] PR. Spalart, WH. Jou, M. Stretlets, and SR. Allmaras. Comments on the feasibility of LES for wings and on the hybrid RANS/LES approach. In *Proceedings of the first AFOSR International Conference on DNS/LES*, 1997.

[11] AS. Zymaris, DI. Papadimitriou, KC. Giannakoglou, and C. Othmer. Continuous adjoint approach to the Spalart-Allmaras turbulence model for incompressible flows. *Computers & Fluids*, 38(8):1528–1538, 2009.

[12] AS. Zymaris, DI. Papadimitriou, KC. Giannakoglou, and C. Othmer. Adjoint wall functions: A new concept for use in aerodynamic shape optimization. *Journal of Computational Physics*, 229(13):5228–5245, 2010.
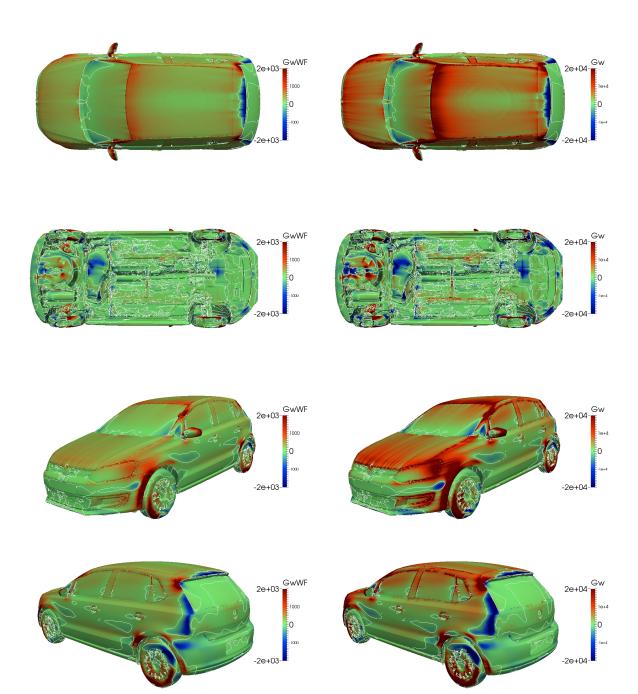
Figure 6: Volkswagen Polo, drag sensitivity map: Sensitivity maps plotted over the surface of the car, as seen from different viewpoints. Red–coloured areas suggest an inward displacement (direction from the fluid to the solid) in order to minimize the objective function, while blue–coloured areas suggest an outward displacement. White isolines indicate sensitivity sign changes (zero sensitivity isolines). Left: sensitivities computed using the proposed method (full differentiation of the turbulence model and utilization of adjoint wall functions). Right: sensitivities based on the "frozen turbulence" assumption. It should be noted that sensitivities based on the 'frozen turbulence" assumption are overestimated by more than an order of magnitude (different colour scale between figures on the left and right).